



# A Simulated Investigation of Ductile Response of GaAs in Single-Point Diamond Turning and Experimental Validation

Pengfei Fan<sup>1</sup> · Fei Ding<sup>1</sup> · Xichun Luo<sup>1</sup> · Yongda Yan<sup>2</sup> · Yanquan Geng<sup>2</sup> · Yuzhang Wang<sup>2</sup>

Received: 28 June 2020 / Revised: 23 September 2020 / Accepted: 9 October 2020 / Published online: 13 November 2020  
© The Author(s) 2020

## Abstract

In this paper, molecular dynamic (MD) simulation was adopted to study the ductile response of single-crystal GaAs during single-point diamond turning (SPDT). The variations of cutting temperature, coordination number, and cutting forces were revealed through MD simulations. SPDT experiment was also carried out to qualitatively validate MD simulation model from the aspects of normal cutting force. The simulation results show that the fundamental reason for ductile response of GaAs during SPDT is phase transition from a perfect zinc blende structure (GaAs-I) to a rock-salt structure (GaAs-II) under high pressure. Finally, a strong anisotropic machinability of GaAs was also found through MD simulations.

**Keywords** Molecular dynamic simulation · Single-point diamond turning · Gallium arsenide · Anisotropy · Ductile response

## 1 Introduction

The last few years have seen a wide exploitation of single-crystal gallium arsenide (GaAs) in photoemitter devices [1], microwave devices [2], hall elements [3], solar cells [4], wireless communications [5], as well as quantum computation [6–8] due to its superior material properties such as higher temperature resistance, and higher electronic mobility and energy gap that outperforms silicon [9–12]. Ultra-precision multiplex 2D or 3D free-form nanostructures are often required on GaAs devices, such as radio frequency power amplifiers and switches used in 5G smart mobile wireless communications [13–15]. Currently, lapping [16, 17] and chemical–mechanical polishing [18–21] have been employed to successfully fabricate planar GaAs wafers. However, they are not competent for the fabrication of 2D or 3D nanostructures. Recently, focused ion beam (FIB) machining has been used to fabricate a hemispherical cavity with highly directional emission on a GaAs workpiece

[22]. However, this approach is not viable for mass production for future commercialization due to the low material removal rate.

In this regard, single-point diamond turning (SPDT) [23–28] becomes a good candidate due to its capability of mass production of 2D and 3D nanostructures with high form accuracy in a single pass. Through establishing machining parameters to meet brittle-to-ductile transition condition, some researchers [29–31] have already successfully obtained nano-smooth machined surfaces on GaAs although it is regarded as a difficult-to-machine brittle material, attributing to its low elastic modulus and fracture toughness. However, so far, the underlying mechanisms of material ductile response and removal during SPDT of single-crystal GaAs have not yet been revealed. This has significantly hampered the development of the SPDT process for the manufacturing of 3D nanostructure on GaAs workpiece.

Molecular dynamic (MD) simulation has been proven to be a reliable theoretical approach to overcome the restriction of experimental observation to study ultra-precision machining brittle materials and has undergone prolific development in recent years [32]. It is capable of simulating structural characteristics of the work material at the atomic scale, which makes it possible to predict the motion and behavior of material atoms. Consequently, some fundamental issues related to nanomachining have been effectively investigated

✉ Xichun Luo  
xichun.luo@strath.ac.uk

<sup>1</sup> Centre for Precision Manufacturing, DMEM, University of Strathclyde, Glasgow, UK

<sup>2</sup> Center for Precision Engineering, Harbin Institute of Technology, Harbin, People's Republic of China

by using the MD approach. For example, Goel et al. [33] firstly revealed that the root cause of ductile response in machining cubic silicon carbide (3C-SiC) was an order-to-disorder transition, i.e., the sp<sup>3</sup>-to-sp<sup>2</sup> structural transformation, during SPDT by using the MD simulation. Subsequently, Xiao et al. [34] employed MD simulation to find that the combination of high-pressure phase transformation (HPPT) and dislocation plasticity was the origin of ductile response during SPDT of 6H-SiC. Additionally, Dai et al. [35] used MD simulation to uncover that the diamond cutting tool with a negative rake angle could experience a lower cutting resistance than the cutting tool with a positive rake angle during machining of single-crystal silicon. Likewise, Chavoshi et al. [36] presented plastic flow behavior of single-crystal silicon in stagnation region during SPDT at elevated temperature by displacement vectors analysis. Recently, Yi et al. [37] carried out a study of MD simulation of nanoscratching process of GaAs using a rigid spherical abrasive tool. The work did not investigate the reason of ductile response, temperature distribution of the cutting zone, and did not carry out experimental validation using a geometric cutting tool. In a word, these works show that MD simulation is a very effective method for investigating the removal mechanism of hard and brittle materials. Therefore, this paper employed MD approach to systematically elucidate an insight of material-removal mechanism for SPDT of single-crystal GaAs along with cutting forces of the diamond cutting tool, visualized temperature distribution of the cutting zone, structural changes of the machined GaAs workpiece, and the anisotropic machinability. In addition, SPDT experiment was conducted to verify the MD simulation results qualitatively. Further SPDT of single-crystal GaAs trial guided by the findings has verified the effectiveness of this simulated study.

## 2 MD Simulation and SPDT Experimental Setups

### 2.1 Simulation Methodology

#### 2.1.1 MD Simulation Model

In this study, an orthogonal MD simulation model for SPDT of single-crystal GaAs, as illustrated in Fig. 1, was established and implemented by using an open source code large-scale atomic/molecular massively parallel simulator (LAMMPS) [38]. The visualization of simulation results was performed by using visual molecular dynamics (VMD) and open visualization tool (Ovito) software [39]. In MD cutting model, the diamond turning tool has a negative rake angle of  $-25^\circ$ , a clearance angle of  $10^\circ$ , and a tool nose radius of 2 nm, as shown in Fig. 1b. Its size is 5.8 nm  $\times$  5.0 nm

$\times$  2.8 nm. To simplify MD simulation and save computational time, the diamond cutting tool was considered as a rigid body without wear and the machining took place with a velocity of 200 m/s on the (0 0 1) surface along the [1 1 0] direction in this study. The dimension of the single-crystal GaAs substrate was 21 nm  $\times$  10 nm  $\times$  13.4 nm containing Newton atoms, thermostat atoms, and boundary atoms, as shown in Fig. 1a, whose initial temperature was maintaining at 300 K by using the Nose–Hoover method [40] running for 50 ps. Periodic boundary condition was applied in the X and Z directions. The simulation was carried out by a depth of cut of 2 nm and a cutting distance of 16 nm and was controlled under the NVE ensemble. The detailed simulation parameters are shown in Table 1.

#### 2.1.2 Adoption of Potential Energy Function

In MD simulation, the force field was made of a hybrid potential function. The C–C atomic interaction in the diamond machining tool was described by the classic Tersoff potential function, which is consistent with the majority of published work on MD simulation of brittle materials [32, 41]. The interaction of single-crystal GaAs workpiece (Ga–Ga, As–As, and Ga–As) was calculated using the updated bond order potentials (BOP) function based on quantum mechanical theory. BOP function, as shown in Eq. (1), is especially suitable for governing the gallium arsenide system because it considers an electron counting potential, which is used to address the distribution of electrons on the GaAs surface. Additionally, the prediction of the structural changes and binding energy trends through BOP function matches experimental observations well [42, 43].

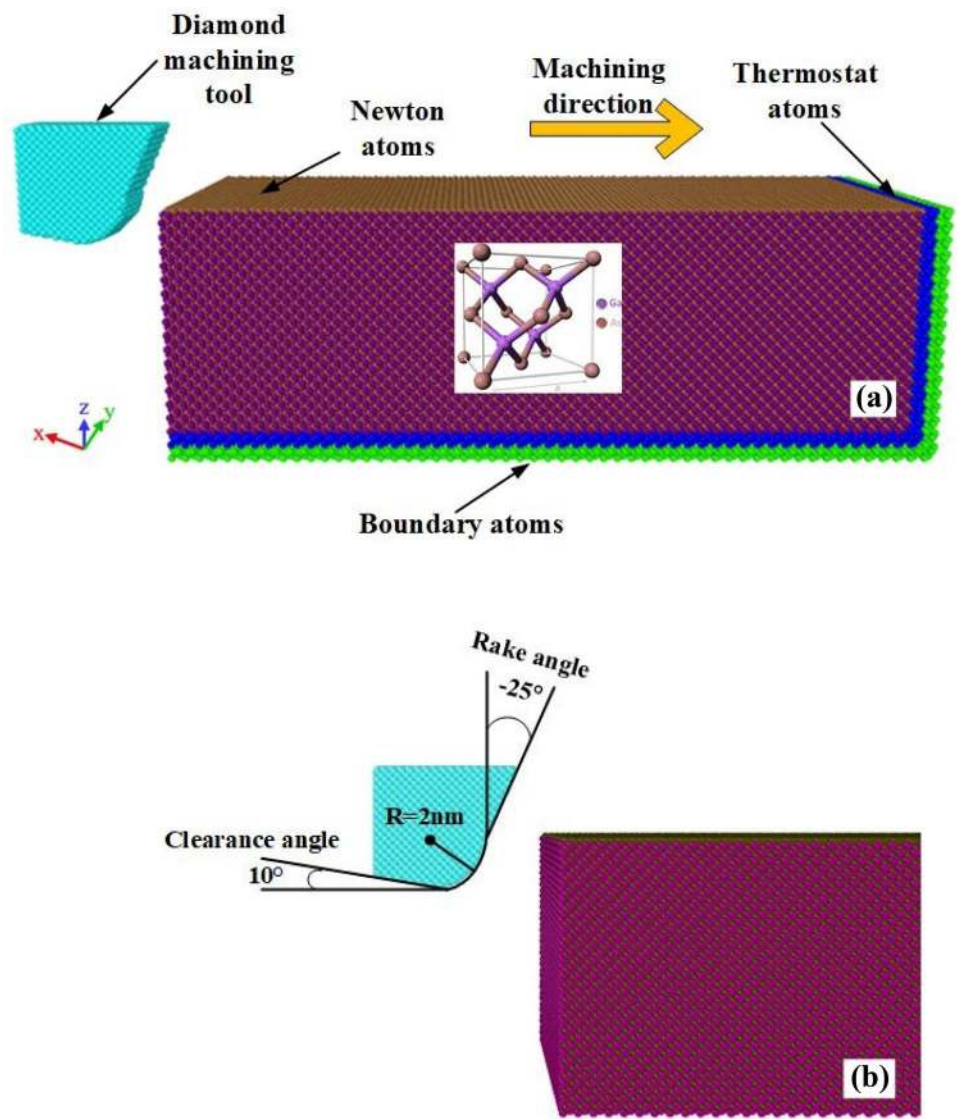
$$E = 1/2 \sum_{i=1}^N \sum_{j=i_1}^{i_N} \varphi_{ij}(r_{ij}) - \sum_{i=1}^N \sum_{j=i_1}^{i_N} \beta_{\sigma,ij}(r_{ij}) \cdot \theta_{(\sigma,ij)} - \sum_{i=1}^N \sum_{j=i_1}^{i_N} \beta_{\pi,ij}(r_{ij}) \cdot \theta_{(\pi,ij)} + U_{\text{prom}} \quad (1)$$

where the  $r_{ij}$  is the distance function for interatomic  $i$  and  $j$   $\varphi_{ij}(r_{ij})$  is the repulsive energy and short-range two-body function,  $\beta_{\sigma,ij}(r_{ij})$  and  $\beta_{\pi,ij}(r_{ij})$  present bond integrals,  $\theta_{\sigma,ij}$  and  $\theta_{\pi,ij}$  refer to specific bond-orders,  $U_{\text{prom}}$  determines the promotion energy about sp-valent systems.

As Ziegler–Biersack–Littmark (ZBL) potential function [44] is suitable to calculate high-energy collisions accurately among C, Ga, and As atoms, it is employed to describe the occurrence of diamond cutting tool collision with GaAs workpiece edge, as follows in Eqs. (2–3).

$$E_{ij}^{\text{ZBL}} = \frac{1}{4\pi\epsilon_0} \frac{Z_i Z_j e^2}{r_{ij}} \varphi(r_{ij}/a) + S(r_{ij}) \quad (2)$$

**Fig. 1** Orthogonal MD simulation model of SPDT on GaAs (0 0 1) surface along the [1 1 0] direction



$$a = \frac{0.46850}{Z_i^{0.23} + Z_j^{0.23}} \quad (3)$$

where  $\epsilon_0$  is the electrical permittivity of vacuum,  $e$  is the electron charge,  $Z_i$  and  $Z_j$  are the nuclear charges of the two types atom,  $r_{ij}$  is identical to mentioned above,  $S(r_{ij})$  refers to a switching function.

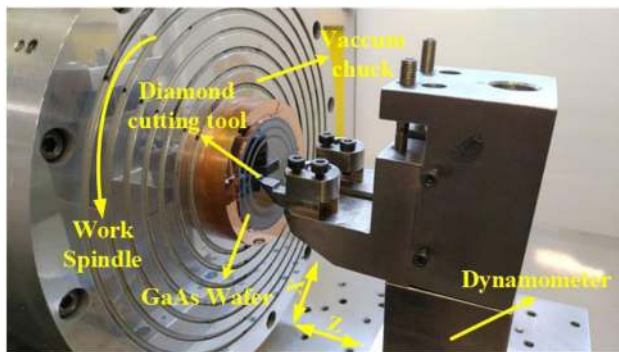
### 2.2 Experimental Setup

In order to verify the MD simulation results, SPDT of GaAs was carried out on an ultra-precision diamond turning machine equipped with air bearing slides and spindle. The experiment setup is shown in Fig. 2. The air bearing spindle has an axial motional error of less than 50 nm. A single-crystal GaAs wafer (diameter of 50 mm, thickness of 5 mm) was glued on a copper fixture which was

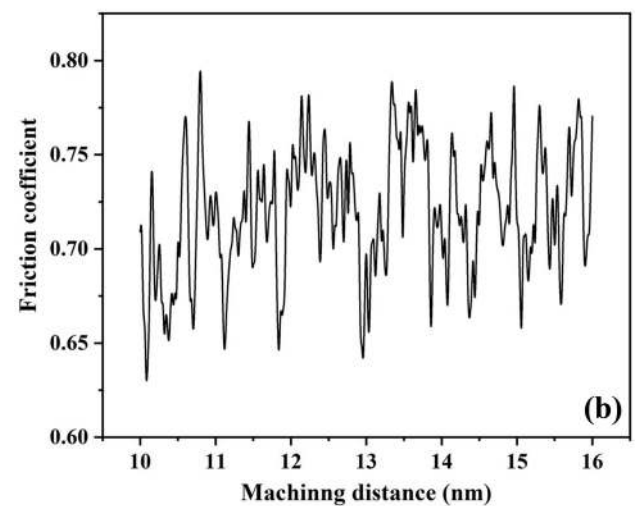
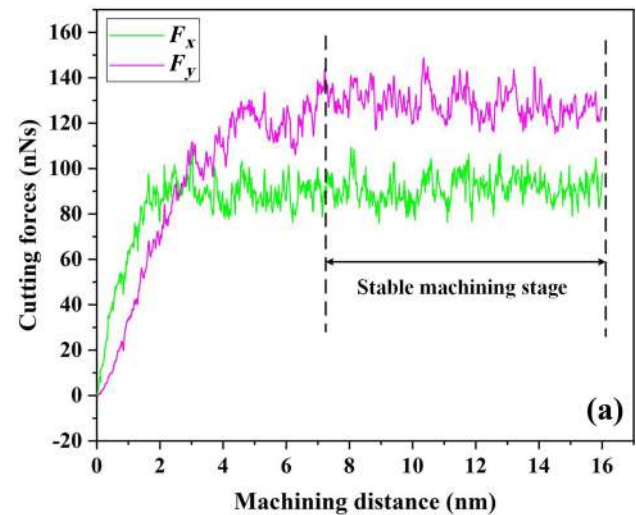
mounted on the vacuum chuck. The cutting direction was along the [1 1 0] direction on the (0 0 1) surface. A cubic lattice structure diamond turning tool with a rake angle of  $-25$  degrees and a clearance angle of  $10$  degrees, which is consistent with the tool geometry used in MD simulation was selected to conduct diamond turning trial. The depth of cut and cutting speed were set as  $10 \mu\text{m}$  and  $1.84 \text{ m/s}$ , respectively. The detailed experimental parameters are shown in Table 2. The cutting force was measured by a dynamometer (Kistler 9129). Finally, the machined GaAs workpiece surface was measured by a white light interferometer (Zygo CP300) after ultrasonic cleaning in a 95 vol% medical alcohol bath. The machining trials were performed on the (0 0 1) surface of the GaAs wafer under a dry cutting condition and at a room temperature of  $20$  degrees in accordance with the MD simulation setup.

**Table 1** MD simulation parameters for SPDT of GaAs

GaAs lattice structure	Zinc-blende
GaAs lattice constant	5.65 Å
Atom numbers of GaAs substrate	190,080
Substrate dimensions	21 nm × 10 nm × 13.4 nm
Machining tool	Cubic diamond
Diamond lattice constant	3.57 Å
Atom numbers of the machining tool	12,085
Machining tool dimensions	5.8 nm × 5.0 nm × 2.8 nm
Rake angle	− 25°
Clearance angle	10°
Tool nose radius	2 nm
Machining depth	2 nm
Machining distance	16 nm
Machining velocity	200 m/s
Machining lattice plane	(0 0 1), (1 1 0), (1 1 1)
Machining direction	[1 1 0]
Equilibration temperature	300 K
Potential functions	Tersoff, BOP, ZBL
Timestep	1 fs

**Fig. 2** Experimental setup of single-point diamond turning of GaAs**Table 2** Diamond turning parameters

Parameters	Unit	Values
Cutting depth	μm	0.3
Cutting speed	m/s	1.84
Feed rate	μm/rev	0.5, 1.0, 1.5
Tool nose radius	mm	5
Tool cutting edge radius	nm	73.79
Tool rake angle	°	− 25
Tool clearance angle	°	10

**Fig. 3** **a** Variation of the cutting forces in the X and Y directions against cutting distances. **b** Variation of friction coefficient of MD simulation results during stable machining stage

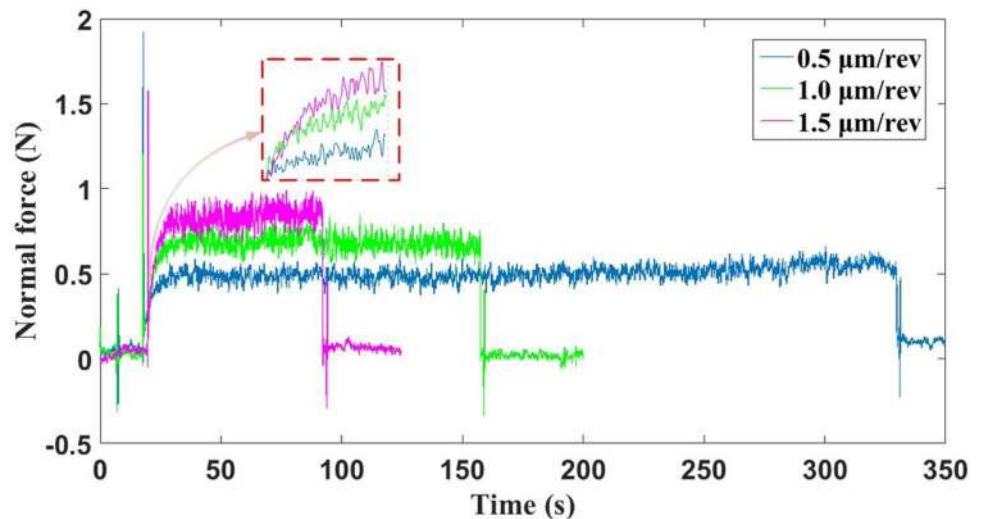
## 3 Results and Discussion

### 3.1 Cutting Forces and Experimental Validation

The cutting force is a pivotal parameter for the study of the SPDT process, as it is directly related to the formation of cutting chip. Figure 3a shows the variation of the cutting forces in the X and Y directions during the cutting process. The tangential cutting force  $F_x$  rose steeply in the first 2 nm of cutting and then fluctuated around 90 nNs at the following 14 nm of cutting with a peak force of 109.373 nNs. The normal force  $F_y$  increased dramatically in the first 7 nm of cutting and also slightly fluctuated at approximately 130 nNs with a maximum value of 149.33 nNs. These data indicate that the cutting chip was generated at the initial 7 nm of cutting and then stabilized in the following 9 nm of cutting.



**Fig. 4** Variations of normal force  $F_y$  at the feed rates of 0.5, 1.0, and 1.5  $\mu\text{m}/\text{rev}$ , respectively



During the fluctuation of cutting force, GaAs's perfect zincblende phase structure was squeezed and deformed by the diamond cutting tool and then the lattice recombined to evolve to a new phase, which will be presented in the following analysis of variation of coordination number (CN) section. In addition, as shown in Fig. 3a, the growth rate of the normal force along the  $Y$  direction is less than that of the tangential force along the  $X$  direction during the chip formation stage but it then became larger than that of the tangential force. This phenomenon is attributed to the use of a diamond cutting tool with a large negative rake angle, which provides a normal cutting force larger than the tangential cutting force. Additionally, the average friction coefficient ( $F_x/F_y$ ) was calculated to be 0.719 during the stable machining stage from the cutting distances of 10–16 nm and its variation is shown in Fig. 3b.

The SPDT of GaAs workpiece experiments were carried out under different feed rates (0.5, 1.0, and 1.5  $\mu\text{m}/\text{rev}$ ). Firstly, the normal force was extracted for each case, as indicated in Fig. 4. It suggests that the normal force of the machining tool experiences a rapid increase in the first 20 s and keeps steady fluctuation after 40 s, which is responsible for the achievement of a stable chip. Consequently, it is obvious to see that the variation trend of experimental normal force in Fig. 4 is consistent with that of MD normal force simulation in Fig. 3a. Hence, the MD simulation results were verified qualitatively to some extent.

### 3.2 GaAs Material Ductile Response

Ductile response of single-crystal GaAs was observed from the MD simulation results, as shown in Fig. 7a, where no cracks or brittle fracture were observed. To reveal the underlying reason for the material ductile response, the average values of the hydrostatic stress at the cutting zone were calculated and are shown in Fig. 5. The hydrostatic stress

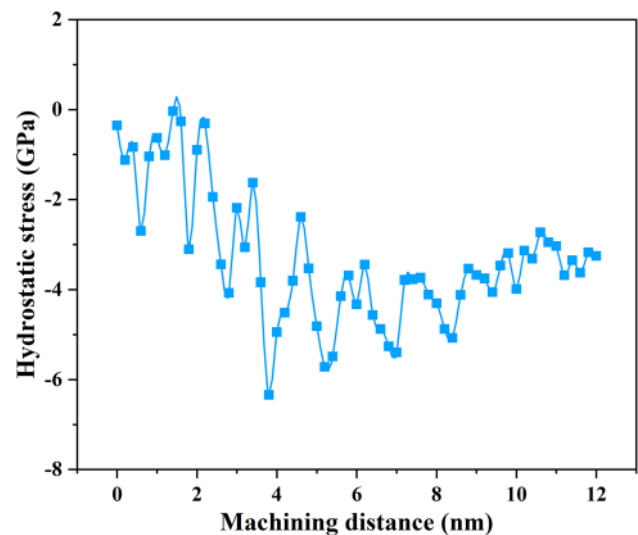


**Fig. 5** Variation of hydrostatic stress value during SPDT

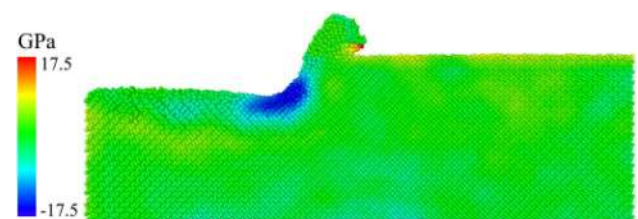


**Fig. 6** Hydrostatic stress distribution of the machined GaAs substrate at a cutting distance of 12 nm

firstly increased rapidly and then fluctuated around 4 GPa during the SPDT process. Additionally, the hydrostatic stress distribution within the machined GaAs substrate, as shown in Fig. 6, revealed that the maximum hydrostatic stress in the cutting zone took place underneath the cutting tool and could rise up to 17.5 GPa. Phase transformation

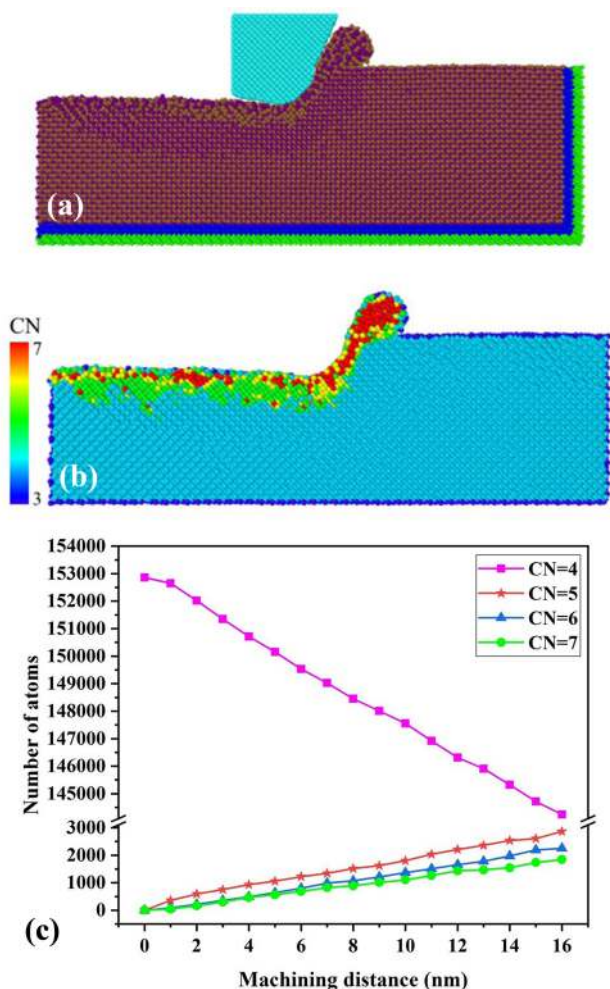


**Fig. 7** **a** Snapshot of MD simulation at cutting distance of 16 nm. **b** Cross-sectional image of CN distribution at the cutting distances of 16 nm. **c** Evolution of various CN atoms against machining distance

of single-crystal GaAs under the same scale of hydrostatic stress was observed in Shigeaki et al.'s experimental work [45]. Therefore, the extremely high hydrostatic stress value during SPDT implies the occurrence of phase transformation of single-crystal GaAs.

To further confirm the occurrence of phase transition of single-crystal GaAs under high hydrostatic stress during SPDT, the coordination number (CN), i.e., the number of the nearest-neighbor atoms around a central atom in a compound, was calculated to characterize the phase transformation of GaAs. The threefold-coordinated value (CN of 3) is indicative of dangling bonds on the surface of GaAs and the fourfold-coordinated value (CN of 4) refers to the intrinsic cubic zinc-blende structure (GaAs-I). The sixfold-coordinated value (CN of 6) presents the rock-salt structure (GaAs-II) and the fivefold-coordinated value (CN of 5) atoms appears the intermediate status between intrinsic zinc blende structure (GaAs-I) and rock-salt structure

(GaAs-II), followed by the amorphous structure of sevenfold-coordinated value (CN of 7) atoms. Figure 7b shows that the machined deformation zone is largely comprised of two kinds of lattice structures: green color atoms with intermediate status CN 5 and yellow color atoms with rock-salt structure (GaAs-II) CN 6, which is attributed to the slow evolution of amorphous structure of the atoms of CN 7 located at the cutting chip. Additionally, the amorphous structure constituted the main part of the cutting chip. The study of temperature distribution among GaAs workpiece during nanomachining process showed that the maximum temperature appeared at the top of the cutting chip, which indicates that the amorphous lattice structure possessed very high lattice deformation energy. As can be seen from Fig. 7c, the number of atoms of CN of four significantly declined, while the atoms with CN of five, CN of six, and CN of seven increased rapidly with the increasing cutting distance. The CN change from four to six implies that the lattice structure of the single-crystal GaAs was transformed from cubic zinc-blende structure to rock-salt structure [46]. In other words, the phase of the single-crystal GaAs was changed from GaAs-I to GaAs-II. Therefore, the reason of the material ductile response of single-crystal GaAs during SPDT is the occurrence of phase transformation of GaAs under extremely high stress, i.e., the so-called high-pressure phase transformation (HPPT) took place. Additionally, neither dislocation nor twinning was observed in this MD simulation study. By contrast, various sorts of dislocations were found out in the MD simulation of diamond turning of Si and SiC [47, 48]. The authors would like to undertake and report a comparison study in the future to reveal the underlying reasons to cause the difference in MD simulation results although they are different brittle materials.

### 3.3 Temperature Distribution During SPDT

Rise of cutting temperature can cause thermal deformation or damage to the workpiece, therefore the cutting temperature is a significant influential factor on the machined surface form accuracy and integrity. In this study, the cutting temperature is calculated by using the following equation,

$$T = \frac{2K.E.}{3NK_b} \quad (4)$$

where the K.E. refers to the kinetic energy of GaAs substrate atoms,  $N$  is the atoms quantity,  $K_b$  represents the Boltzmann constant. The temperature was averaged over a cubic zone with a length of 10 Å. A defined elemental atomic volume (16 nm × 2 nm × 3 nm) was set to the primary cutting zone. A dramatic rise of cutting temperature with the increase of cutting distance was observed in the diagram of the variation of cutting temperature shown in

**Fig. 8** **a** Temperature distribution on the GaAs workpiece after 16 nm of cut. **b** Increase of temperature during SPDT machining

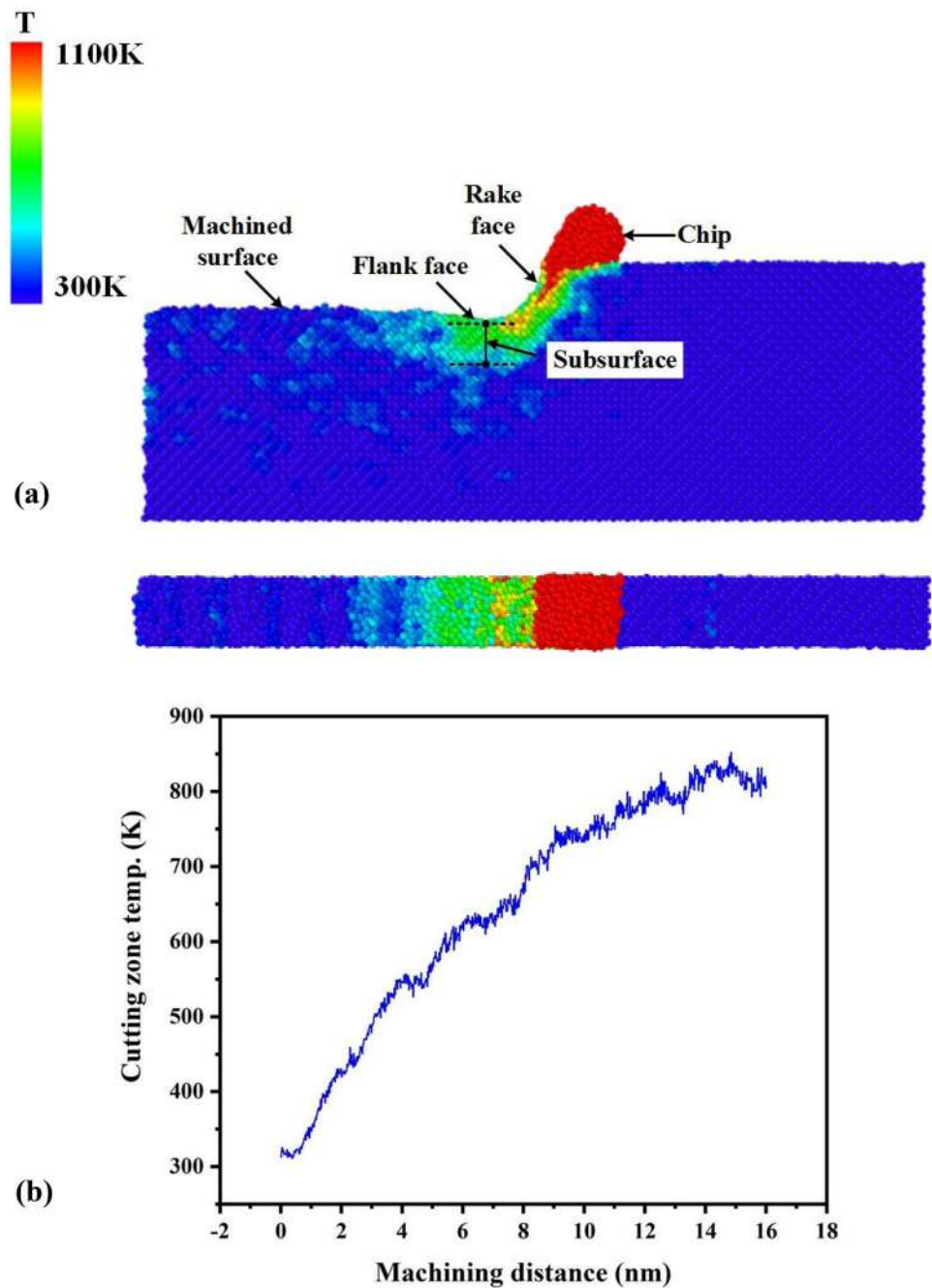


Fig. 8b. The cutting temperature reached a maximum value of 851.86 K after the cutting distance of 15 nm. Figure 8a illustrates the temperature distribution using various color zones. The same phenomenon has been observed on other ductile and brittle materials such as Cu, Al, and Si materials [40, 41]. According to temperature distribution, the highest temperature appeared at the top of the chip, which is up to 1100 K. This is because the top of the chip experienced the most serious lattice deformation, which could possess the

maximum transformation lattice energy. Furthermore, the diamond tool rake face and flank face also showed extremely high temperatures, nearly 900 and 700 K, respectively, since the rake face pressed against the GaAs atoms and friction occurred between the flank face and the machined GaAs surface. Additionally, the subsurface of the machine GaAs at 2 nm underneath the flank face showed a high temperature of approximately 700 K. Finally, most of the atoms beside the substrate edge could keep an almost stable temperature 300 K, which benefited from the heat dissipation of the thermostat layer atoms.



### 3.4 The Influence of Crystalline Orientation

This paper analyzes the effect of crystalline orientation on the cutting chip, sidewall morphology, and friction coefficient among typical crystal orientations, including the (0 0 1) surface along the  $[1\ 1\ 0]$  cutting direction, (1 1 0) surface along the  $[0\ 0\ 1]$  cutting direction, and (1 1 1) surface along

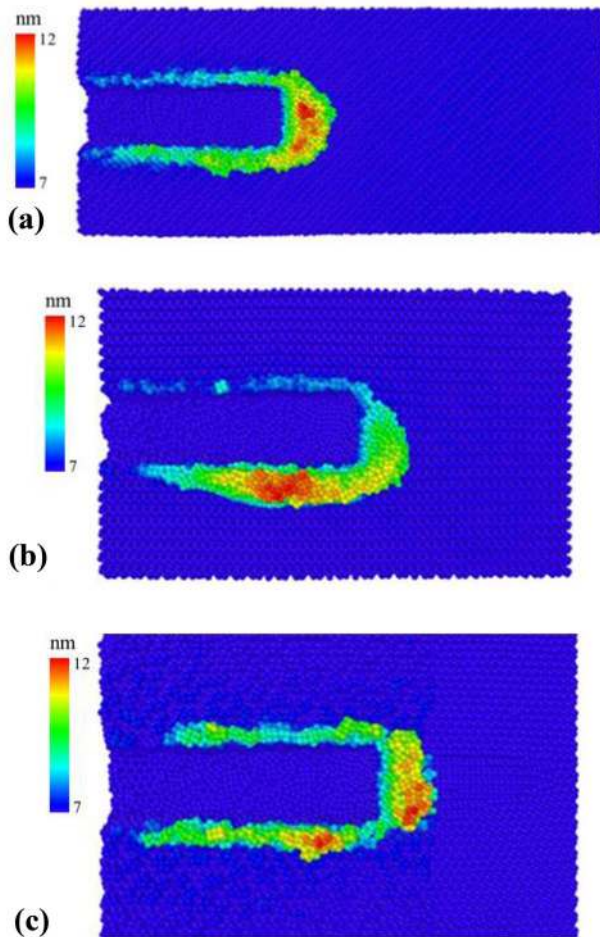


**Fig. 9** The colored morphology of cutting chip and sidewall pile-up during along the Y direction **a** GaAs (0 0 1), **b** GaAs (1 1 0), **c** GaAs (1 1 1)

the  $[1\ \bar{1}\ 0]$  cutting direction. According to Figs. 9 and 10, it is clear to see that the GaAs atoms piled up on both sides of the nanogroove when cutting the (0 0 1) and (1 1 1) surfaces. Furthermore, when cutting the (1 1 1) surface, the GaAs atoms were evenly distributed on both sides, while for cutting the (0 0 1) surface, more atoms were piled up on the right side than the left. Almost all the removed atoms were piled up on the right side for machining (1 1 0) surface. Meanwhile, the left-hand side atoms could have more atom pile-ups than the right-hand side when cutting along the opposite direction  $[0\ 0\ \bar{1}]$  on (1 1 0) surface, as shown in Fig. 10c. This occurrence might be attributed to different atomic density and inter-atomic distance in different GaAs crystal surfaces.

Additionally, the cutting forces and friction coefficients were calculated for three different kinds of crystal surfaces. The results are shown in Table 3. The minimum friction coefficient of 0.630 was found when cutting the (1 1 1) face along the  $[1\ \bar{1}\ 0]$  direction, which means the SPDT process has the least resistance in this crystalline orientation and cutting direction combination. The maximum friction coefficient of 0.719 was found when cutting the GaAs (0 0 1) surface along the  $[1\ 1\ 0]$  direction. Cutting the (1 1 0) surface along the  $[0\ 0\ 1]$  direction shows the intermediate friction coefficient of 0.680. The results suggested that the  $[1\ 1\ 0]$  direction is the hardest machining direction on the (0 0 1) surface. This finding is consistent with the conclusion drawn in the experimental study on circumferential distribution of material brittle fracture index of single-crystal GaAs by Chen et al. [31]. In theory, if the GaAs material showed ductile response on the difficult-to-cut surface and cutting

**Table 3** The average value of tangential force, normal force, and friction coefficient during SPDT on different crystalline orientations

	$F_x$ (nNs)	$F_y$ (nNs)	FC
(0 0 1)	91.56	127.35	0.719
(1 1 0)	82.27	120.99	0.680
(1 1 1)	66.35	105.31	0.630

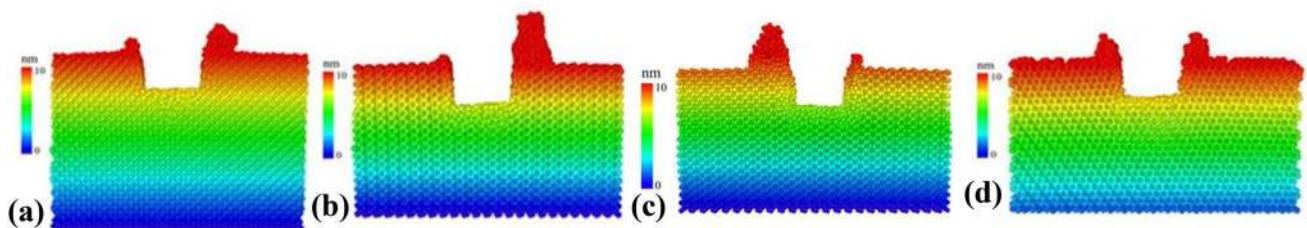
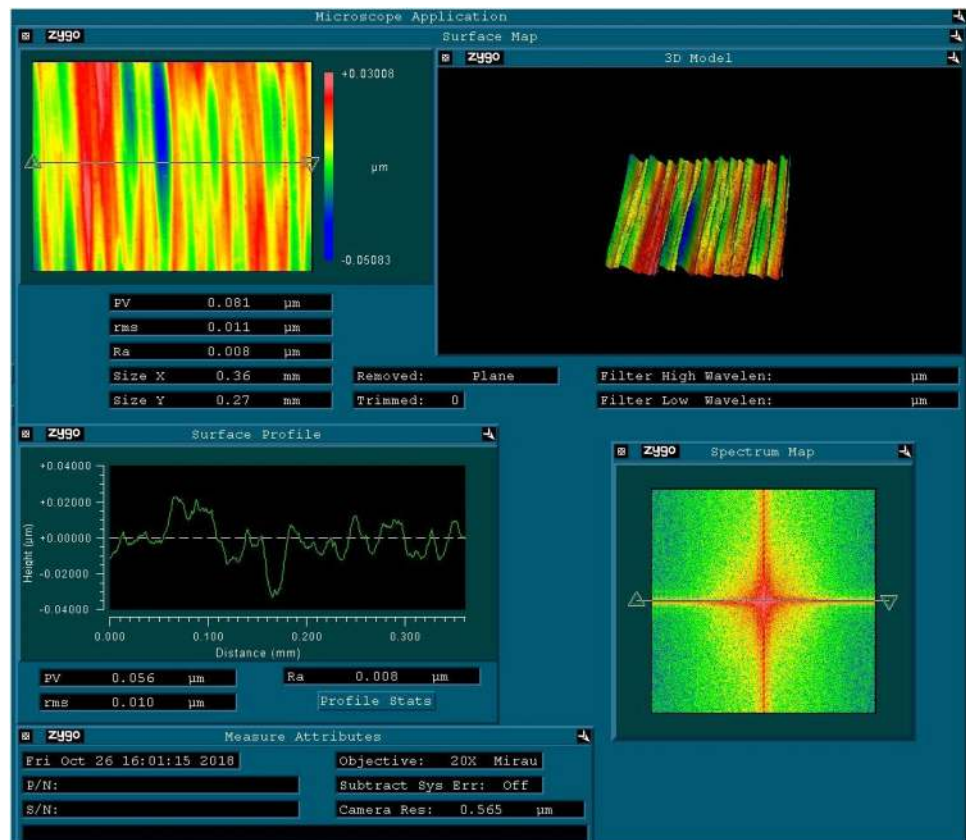


**Fig. 10** The pile-up of the sidewall during SPDT along the Y direction **a** GaAs (0 0 1), **b** GaAs (1 1 0) along  $[0\ 0\ 1]$ , **c** GaAs (1 1 0) along  $[0\ 0\ \bar{1}]$ , **d** GaAs (1 1 1)



**Fig. 11** Measured machined surface of GaAs in the SPDT experiment



direction, brittle fracture-free machined surfaces could therefore be achieved in other crystal orientations and cutting direction under the same machining parameters. In this study, we selected the most difficult-to-machine (0 0 1) surface to carry out SPDT experiments along the most difficult-to-machine cutting direction [1 1 0]. The experimental result showed a nano-smooth machined GaAs surface finish with a surface roughness  $R_a$  of 8 nm could be obtained when using a feed rate of 0.5  $\mu\text{m}/\text{rev}$ , a spindle speed of 800 rpm, and a depth of cut 0.3  $\mu\text{m}$ , which is shown in Fig. 11.

## 4 Conclusions

In this work, both MD simulations and SPDT experiments have been employed to investigate atomistic aspects of ductile response of single-crystal GaAs material. The conclusions can be drawn as follows:

1. The SPDT is accompanied by a sharp rise in temperature in the cutting zone. The generated highest temperature is located at the cutting chip, in which the temperature can reach up to 1100 K. Furthermore, the rake face and flank face also have extremely high temperatures of nearly 900 and 700 K, respectively.
2. The underlying reason for the single-crystal GaAs ductile response during SPDT process is the high-pressure phase transformation (HPPT), in which the intrinsic zinc-blende phase structure GaAs-I of single-crystal GaAs transformed to a rock-salt phase structure GaAs-II under high hydrostatic stress. In addition, the intermediate phase structure and rock-salt phase structure dominate the machined deformation zone while the amorphization structure mainly consists of the formed chip.
3. Single-crystal GaAs shows the strong anisotropic machinability during SPDT. When cutting the (0 0 1) surface along the [1 1 0] direction, the simulated morphology shows that more atoms pile up on the right side than the left side, while GaAs atoms are well distributed on both sides when cutting the (1 1 1) surface along the [1  $\bar{1}$  0] direction. With regards to cutting the (1 1 0) surface along the [0 0 1] direction, almost all piled-up GaAs atoms appeared on the right side. The maximum friction coefficient is found when cutting the GaAs (0 0 1) surface along the [1 1 0] direction while cutting the (1 1 1) surface along the [1  $\bar{1}$  0] direction possessed the minimum friction coefficient. The friction coefficient when cutting the (1 1 0) surface along the [0 0 1] direction is intermediate among these three typical crystalline orientations and cutting-direction combinations.

**Acknowledgements** The authors would like to thank EPSRC (EP/K018345/1 and EP/T024844/1) and the Royal Society-NSFC international exchange programme (IECN\NSFC\181474) for providing financial support for this research. The authors also acknowledge the use of the EPSRC (EP/K000586/1) funded ARCHIE-WeSt High-Performance Computer at the University of Strathclyde for the MD simulation study.

**Data Availability** All data underpinning this publication are openly available from the University of Strathclyde KnowledgeBase at <https://doi.org/10.15129/746765d8-0cd3-4320-ac8e-fe4d3192e90a>.

**Open Access** This article is licensed under a Creative Commons Attribution 4.0 International License, which permits use, sharing, adaptation, distribution and reproduction in any medium or format, as long as you give appropriate credit to the original author(s) and the source, provide a link to the Creative Commons licence, and indicate if changes were made. The images or other third party material in this article are included in the article's Creative Commons licence, unless indicated otherwise in a credit line to the material. If material is not included in the article's Creative Commons licence and your intended use is not permitted by statutory regulation or exceeds the permitted use, you will need to obtain permission directly from the copyright holder. To view a copy of this licence, visit <http://creativecommons.org/licenses/by/4.0/>.

## References

- Blankemeier L, Rezaeifar F, Garg A, Kapadia R (2019) Integrated photonics for low transverse emittance, ultrafast negative electron affinity GaAs photoemitters. *J Appl Phys* 126(3):033102
- Nanayakkara TR et al (2018) Electron heating induced by microwave photoexcitation in the GaAs/AlGaAs two-dimensional electron system. *Phys Rev B* 98(3):1–6
- Kunets VP et al (2008) Low thermal drift in highly sensitive doped channel Al<sub>0.3</sub>Ga<sub>0.7</sub>As/GaAs/In<sub>0.2</sub>Ga<sub>0.8</sub>As micro-Hall element. *J Mater Sci Mater Electron* 19(8–9):776–782
- Mazouz H, Logerais PO, Belghachi A, Riou O, Delalex F, Durastanti JF (2015) Effect of electron irradiation fluence on the output parameters of GaAs solar cell. *Int J Hydrog Energy* 40(39):13857–13865
- Blin S et al (2013) Wireless communication at 310 GHz using GaAs high-electron-mobility transistors for detection. *J Commun Netw* 15(6):559–568
- Li HO et al (2015) Conditional rotation of two strongly coupled semiconductor charge qubits. *Nat Commun* 6:1–9
- Cao G et al (2013) Ultrafast universal quantum control of a quantum-dot charge qubit using Landau–Zener–Stückelberg interference. *Nat Commun* 4:1–7
- Shi Z et al (2014) Fast coherent manipulation of three-electron states in a double quantum dot. *Nat Commun* 5:1–5
- Cheng W, Hu CL, Jiao GC, Miao Z, Zhang N (2013) Analyses the character of GaAs photocathode by diffraction curve from spectrophotometer. *Key Eng Mater* 552:287–291
- Kudrawiec R, Misiewicz J, Fisher M, Forchel A (2004) Optical properties of GaInNas/GaAs quantum wells: character of optical transitions and carrier localisation effect. *Phys Status Solidi Appl Res* 201(2):364–367
- Mäder KA, Wang LW, Zunger A (1995) Electronic consequences of random layer-thickness fluctuations in AlAs/GaAs superlattices. *J Appl Phys* 78(11):6639–6657
- Gangopadhyay A, Maros A, Faleev N, Smith DJ (2019) Strain relaxation in low-mismatched GaAs/GaAs<sub>1-x</sub>Sb<sub>x</sub>/GaAs heterostructures. *Acta Mater* 162:103–115
- Ahn HJ, Il Chang W, Kim SM, Park BJ, Yook JM, Eo YS (2019) 28 GHz GaAs pHEMT MMICs and RF front-end module for 5G communication systems. *Microw Opt Technol Lett* 61(4):878–882
- Nitesh RS, Rajendran J, Ramiah H, Abd sssssManaf A (2018) A 700MHz to 2.5GHz cascode GaAs power amplifier for multi-band pico-cell achieving 20 dB gain, 40 dBm to 45 dBm OIP3 and 66% peak PAE. *IEEE Access* 6:818–829
- Florencio Díaz R, Rodríguez Boix R, Carrasco Yépez F, Encinar Garcinuño J, Barba Gea M, Pérez Palomino G (2014) Broadband reflect arrays made of cells with three coplanar parallel dipoles. *Microw Opt Technol Lett* 56(3):748–753
- Sasani K, Abbasi SP, Sabrlouy Kolian B, Zabihi MS, Sabbaghzadeh J (2011) Relationship between concentration, time and surface roughness of GaAs wafer in lapping process: an experimental investigation. In: 2011 symposium on photonics and optoelectronics, SOPO 2011, pp 1–4
- Prakash SJ, Tyagi R, Gupta A (2011) Backside thinning of GaAs wafer by lapping using DOE approach. In: India international conference on power electronics, IICPE 2010, pp 1–4
- Mcmeekin SG, Robertson M, Mcgheeb L, Winfield JM (1992) Chemimechanical polishing of gallium arsenide to subnanometre surface finish. *J Mater Chem* 2(3):367–368
- Wu YH, Chang L (2010) Chemical polishing method of GaAs specimens for transmission electron microscopy. *Micron* 41(1):20–25
- Antwi EK, Liu K, Wang H (2018) A review on ductile mode cutting of brittle materials. *Front Mech Eng* 13(2):251–263
- Venkatesh VC, Inasaki I, Toenshof HK, Nakagawa T, Marinescu ID (1995) Observations on polishing and ultraprecision machining of semiconductor substrate materials. *CIRP Ann Manuf Technol* 44(2):611–618
- Ma Y, Ballesteros G, Zajac JM, Sun J, Gerardot BD (2015) Highly directional emission from a quantum emitter embedded in a hemispherical cavity. *Opt Lett* 40(10):2373
- Blake PN, Scattergood RO (1990) Ductile-regime machining of germanium and silicon. *J Am Ceram Soc* 73(4):949–957
- Li Z, Zhang X (2017) Subsurface deformation of germanium in ultra-precision cutting: characterization of micro-Raman spectroscopy. *Int J Adv Manuf Technol* 91(1–4):213–225
- Goel S, Luo X, Reuben RL (2013) Wear mechanism of diamond tools against single-crystal silicon in single-point diamond turning process. *Tribol Int* 57:272–281
- Goel S, Luo X, Comley P, Reuben RL, Cox A (2013) Brittle-ductile transition during diamond turning of single-crystal silicon carbide. *Int J Mach Tools Manuf* 65:15–21
- Mir A, Luo X, Cheng K, Cox A (2018) Investigation of influence of tool rake angle in single-point diamond turning of silicon. *Int J Adv Manuf Technol* 94(5–8):2343–2355
- Jasinevicius RG (2006) Influence of cutting conditions scaling in the machining of semiconductors crystals with single-point diamond tool. *J Mater Process Technol* 179(1–3):111–116
- Fang ZJYFZ (1999) Ultra-precision cutting for gallium arsenide. In: Proceedings of the ASPE annual meeting, pp 62–66
- Wang S, Pirouz P (2007) Mechanical properties of undoped GaAs. II: the brittle-to-ductile transition temperature. *Acta Mater* 55(16):5515–5525
- Chen J, Luo X, Ding F, Rao X, Zhang J (2020) Fundamental study of diamond turning of single-crystal gallium arsenide. *Precis Eng* 62:71–82

32. Goel S, Luo X, Agrawal A, Reuben RL (2015) Diamond machining of silicon: a review of advances in molecular dynamics simulation. *Int J Mach Tools Manuf* 88:131–164
33. Goel S, Luo X, Reuben RL, Bin Rashid W (2011) Atomistic aspects of ductile responses of cubic silicon carbide during nanometric cutting. *Nanoscale Res Lett* 6:1–9
34. Xiao G, To S, Zhang G (2015) The mechanism of ductile deformation in ductile regime machining of 6H SiC. *Comput Mater Sci* 98:178–188
35. Dai H, Chen G, Fang Q, Yin J (2016) The effect of tool geometry on subsurface damage and material removal in nanometric cutting single-crystal silicon by a molecular dynamics simulation. *Appl Phys A Mater Sci Process* 122(9):1–16
36. Chavoshi SZ, Goel S, Luo X (2015) Molecular dynamics simulation investigation on the plastic flow behaviour of silicon during nanometric cutting. *Model Simul Mater Sci Eng* 24(1):015002
37. Yi D, Li J, Zhu P (2018) Study of nanoscratching process of GaAs using molecular dynamics. *Crystals* 8(8):321
38. Plimpton SJ (1995) Fast parallel algorithms for short range molecular dynamics. *J Comput Phys* 117:1–19
39. Stukowski A (2010) Visualization and analysis of atomistic simulation data with OVITO—the open visualization tool. *Model Simul Mater Sci Eng* 18(1):015012
40. Nose S (1984) A unified formulation of the constant temperature molecular-dynamics methods. *J Chem Phys* 81:511–519
41. Tersoff J (1989) Modeling solid-state chemistry: interatomic potentials for multicomponent systems. *Phys Rev B* 39(8):5566–5568
42. Ward DK, Zhou XW, Wong BM, Doty FP, Zimmerman JA (2012) Analytical bond-order potential for the cadmium telluride binary system. *Phys Rev B Condens Matter Mater Phys* 85(11):1–19
43. Pettifor DG, Oleinik II (2002) Analytic bond-order potential for open and close-packed phases. *Phys Rev B Condens Matter Mater Phys* 65(17):1–4
44. Ziegler JF, Ziegler MD, Biersack JP (2010) SRIM: the stopping and range of ions in matter (2010). *Nucl Instrum Methods Phys Res Sect B Beam Interact Mater Atoms* 268(11–12):1818–1823
45. Ono S, Kikegawa T (2018) Phase transformation of GaAs at high pressures and temperatures. *J Phys Chem Solids* 113:1–4
46. Besson JM, Itié JP, Polian A, Weill G, Mansot JL, Gonzalez J (1991) High-pressure phase transition and phase diagram of gallium arsenide. *Phys Rev B* 44(9):4214–4234
47. Chavoshi SZ, Xu S, Luo X (2016) Dislocation-mediated plasticity in silicon during nanometric cutting: a molecular dynamics simulation study. *Mater Sci Semicond Process* 51:60–70
48. Chavoshi SZ, Luo X (2016) Molecular dynamics simulation study of deformation mechanisms in 3C-SiC during nanometric cutting at elevated temperatures. *Mater Sci Eng A* 654:400–417



**Pengfei Fan** is a Doctoral candidate of DMEM at the University of Strathclyde, UK. His research interests include ultra precision manufacturing, nanofabrication and multiscale simulation technique.



**Fei Ding** is a Doctoral candidate of DMEM at the University of Strathclyde, UK. His research interests include precision motion control, advanced manufacturing techniques and ultra-precision machine tool design.



**Dr. Xichun Luo** is a Professor in ultra precision manufacturing and technical director of Centre for Precision Manufacturing at the University of Strathclyde. He is Fellow of the International Society for Nanomanufacturing. His research interests include ultra precision machining, micromachining and nanomanufacturing with more than 100 papers in peer-reviewed journals and conferences.



**Dr. Yongda Yan** is a professor in School of Mechatronics Engineering, Center for Precision Engineering and Key Laboratory of Micro-systems and Micro-structures Manufacturing of Ministry of Education of Harbin Institute of Technology. He is a research affiliate of CIRP since 2013. His main research field is the micro/nano mechanical machining techniques and their applications. He received his M.S. and Ph.D. degrees in mechanical engineering from Harbin Institute of Technology

in 2001 and 2007, respectively.





**Dr. Yanquan Geng** is an associate professor in Center for Precision Engineering and Key Laboratory of Micro-systems and Micro-structures Manufacturing of Ministry of Education of Harbin Institute of Technology. He received his B.S., M.S. and Ph.D. degrees in mechanical engineering from Harbin Institute of Technology in 2009, 2011 and 2016. After joining Prof. Yongda Yan's group since 2011, he started his research on the AFM-based nanomachining technique and related

applications.



**Yuzhang Wang** is a Doctoral candidate of school of mechanical engineering at the Harbin Institute of Technology. His research interests include nanofabrication, precision manufacturing techniques and system control.